Charged nanograins in the Enceladus plume

T. W. Hill,[1] M. F. Thomsen,[2] R. L. Tokar,[2] A. J. Coates,[3] G. R. Lewis,[3] D. T. Young,[4] F. J. Crary,[4] R. A. Baragiola,[5] R. E. Johnson,[5] Y. Dong,[1] R. J. Wilson,[6] G. H. Jones,[3] J.-E. Wahlund,[7] D. G. Mitchell,[8] and M. Horányi[6]

Received 1 October 2011; revised 15 March 2012; accepted 16 March 2012; published 4 May 2012.

[1] There have been three Cassini encounters with the south-pole eruptive plume of Enceladus for which the Cassini Plasma Spectrometer (CAPS) had viewing in the spacecraft ram direction. In each case, CAPS detected a cold dense population of heavy charged particles having mass-to-charge (m/q) ratios up to the maximum detectable by CAPS ($\sim 10^4$ amu/e). These particles are interpreted as singly charged nanometer-sized water-ice grains. Although they are detected with both negative and positive net charges, the former greatly outnumber the latter, at least in the m/q range accessible to CAPS. On the most distant available encounter (E3, March 2008) we derive a net (negative) charge density of up to ~ 2600 e/cm^3 for nanograins, far exceeding the ambient plasma number density, but less than the net (positive) charge density inferred from the RPWS Langmuir probe data during the same plume encounter. Comparison of the CAPS data from the three available encounters is consistent with the idea that the nanograins leave the surface vents largely uncharged, but become increasingly negatively charged by plasma electron impact as they move farther from the satellite. These nanograins provide a potentially potent source of magnetospheric plasma and E-ring material.

Citation: Hill, T. W., et al. (2012), Charged nanograins in the Enceladus plume, *J. Geophys. Res.*, *117*, A05209, doi:10.1029/2011JA017218.

1. Introduction

[2] Enceladus is a small icy satellite (radius $R_E \approx 252$ km) that orbits Saturn at a planet-centered distance of about 3.95 R_S (Saturn's equatorial radius $R_S \approx 60{,}300$ km). Despite its small size, Enceladus is geologically active, for reasons that are not understood. Evidence for this activity includes linear "tiger stripe" surface features at high southern latitudes that are much warmer than the surrounding surface in Cassini Composite Infrared Spectrometer (CIRS) images [*Spencer et al.*, 2006], and associated eruptive jets or plumes of micrometer-size water-ice dust particles that extend at least several R_E into space. The micron-size dust was detected directly by the Cassini Cosmic Dust Analyzer (CDA) instrument [*Spahn et al.*, 2006], and is clearly visible in forward-scattered sunlight images from the Cassini Imaging Science Subsystem (ISS) reported by *Porco et al.* [2006]. These plumes also contain copious amounts of neutral-water vapor, as detected both remotely by the Cassini Ultraviolet Imaging Spectrometer (UVIS) [*Hansen et al.*, 2006] and in situ by the Cassini Ion and Neutral Mass Spectrometer (INMS) [*Waite et al.*, 2006]. The plumes also contain negative water-cluster molecular ions [*Coates et al.*, 2009], positive water-group ions [*Tokar et al.*, 2009], and charged nanometer-sized grains [*Jones et al.*, 2009], all detected in situ by the Cassini Plasma Spectrometer (CAPS), as well as a cold dense plasma detected in situ by the Cassini Radio and Plasma Wave Science – Langmuir Probe (RPWS-LP) instrument [*Shafiq et al.*, 2011]. The charged nanometer-size grains ("nanograins") detected by CAPS during plume encounters are the subject of this paper.

[3] The Cassini spacecraft has made several targeted encounters with the Enceladus plume. Of these, three provided ram pointing (in the direction of spacecraft motion) for the CAPS instrument, encounters E3 (12 Mar 2008), E5 (9 Oct 2008), and E7 (2 Nov 2009); see Figure 1. All three passed very close to the plume axis (≈the south polar axis of Enceladus). Ram pointing is a requirement for CAPS detection of these cold, heavy charged grains. Here we

[1]Physics and Astronomy Department, Rice University, Houston, Texas, USA.
[2]Space Science and Applications, Los Alamos National Laboratory, Los Alamos, New Mexico, USA.
[3]Mullard Space Science Laboratory, University College London, Dorking, UK.
[4]Space Science and Engineering Division, Southwest Research Institute, San Antonio, Texas, USA.
[5]School of Engineering and Applied Science, University of Virginia, Charlottesville, Virginia, USA.
[6]Laboratory for Atmospheric and Space Physics, University of Colorado at Boulder, Boulder, Colorado, USA.
[7]Swedish Institute of Space Physics, Uppsala, Sweden.
[8]Applied Physics Laboratory, Johns Hopkins University, Laurel, Maryland, USA.

Corresponding Author: T. W. Hill, Physics and Astronomy Department, Rice University, MS 108, PO Box 1892, Houston, TX 77251-1892, USA. (hill@rice.edu)

0148-0227/12/2011JA017218

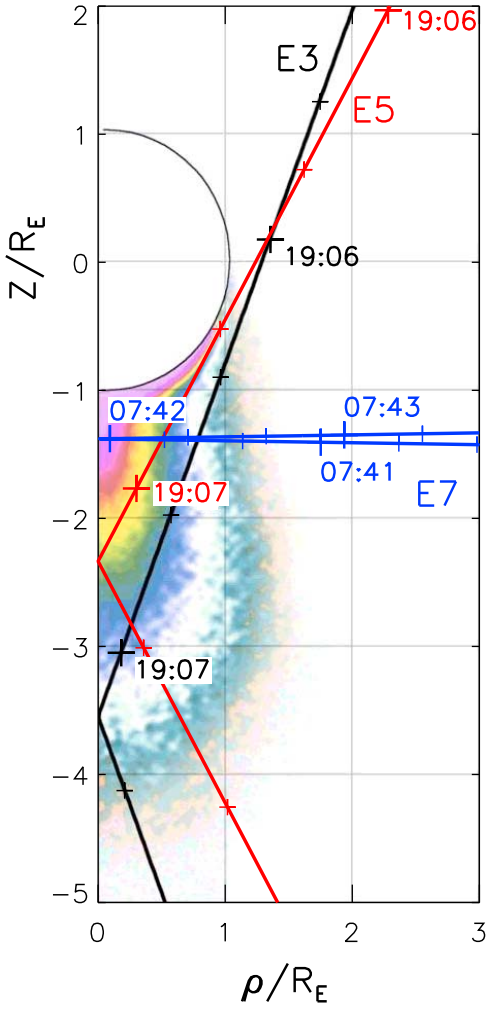

Figure 1. The three Cassini Enceladus plume encounters to date that have had CAPS ram pointing, in a (ρ,z) cylindrical coordinate system aligned with the polar axis of Enceladus. Times (UT) are marked at 20-s intervals and labeled at 1-min intervals. The background color is a depiction of the intensity of the visible dust signal detected by the Cassini Imaging Science Subsystem (http://saturn.jpl.nasa.gov/photos/imagedetails/index.cfm?imageId =2985).

present our analysis of CAPS nanograin observations during the E3, E5, and E7 encounters and our expectations for future encounters.

2. Observations

[4] CAPS contains three detector systems, an Electron Spectrometer (ELS), an Ion Mass Spectrometer (IMS), and an Ion Beam Spectrometer (IBS). The ELS provides electrostatic energy-per-charge (E/q) analysis of electrons in the range 0.7–28,800 eV/e, and any other negatively charged particles that fall in the same E/q range, e.g., the cold heavy negative ions discovered in the ionosphere of Titan [*Coates et al.*, 2007] and in the Enceladus plume [*Coates et al.*, 2009] that are boosted into the ELS energy range by the spacecraft ram velocity. The IMS provides electrostatic E/q analysis of positive ions in the range 1–34,700 eV/e, and also includes a time-of-flight (TOF) system for composition (m/q) analysis. Both ELS and IMS have fan-shaped fields of view spanning 5° × 160° (ELS) and 8° × 160° (IMS), divided into eight contiguous angular sectors of 5° × 20° (ELS) and 8° × 20° (IMS). The IBS detects ions in a specifiable subset of the IMS E/q range, but has a much narrower field of view designed to resolve highly collimated beams like the solar wind. Because Cassini is a non-spinning spacecraft, the detectors are mounted on an actuator platform that, when activated, provides a 180° sweep in the azimuthal direction, but the actuator was deactivated during the three encounters discussed here in order to provide steady viewing of the spacecraft ram direction, which appears in anode 5 (the fifth of the eight angular sectors) on the E3 and E5 encounters, and in anode 4 on E7. In this paper we utilize data from ELS and IMS. Accumulation times were insufficient for TOF analysis, and IBS signals, when available, were consistent with the corresponding IMS signals. For a further description of CAPS, see *Young et al.* [2004].

[5] Figure 2 shows counting-rate spectrograms from ELS (Figure 2, top) and IMS (Figure 2, bottom) for a five-minute interval surrounding the E3 encounter on 12 Mar 2008. Figure 3 shows the same thing for the E5 encounter on 9 Oct 2008. The counting rate is roughly proportional to particle energy flux. The ELS counting rate is from anode 5, one of the two angular sectors (4 and 5) that border on the spacecraft ram direction, while the IMS counting rate is summed over all anodes to enhance the signal-to-noise ratio, but is dominated by the anodes closest to the ram direction for the feature of interest here. For both encounters, the nanograin signature occurs near the top of the CAPS E/q range, above a few 100 eV/e for ELS and a few 1000 eV/e for IMS. The lower-E/q signals are from ambient plasma and locally produced ions, as discussed by *Coates et al.* [2009] for negative ions and *Tokar et al.* [2009] for positive ions. The nanograin populations, discussed by *Jones et al.* [2009] and *Coates et al.* [2010], obviously extend well beyond the upper limit of the CAPS E/q ranges for both ELS and IMS. The nanograin signature in the IMS spectrogram is similar in shape to that in the ELS spectrogram but is shifted higher in energy and peaks later in time.

[6] Figure 4 shows sample spectra of counting rates versus E/q for negative (ELS) and positive (IMS) particles on the E3 encounter, at times near the respective peaks of the nanograin flux. Figure 5 shows the same thing for the E5 encounter. The times of flux maxima cannot be determined precisely because much if not most of the flux occurs above the top of the CAPS E/q ranges, and the peak times in any case differ significantly between positive and negative grains. The spectra shown are typical of those observed near the flux peaks. The upper horizontal scales show the corresponding m/q range in units of H_2O molecular masses per elementary charge (18 amu/e), assuming $E = mv^2/2$ where v = spacecraft speed relative to Enceladus (see below). These spectra are vertical 2D slices through the 3D spectrograms of Figures 2 and 3, respectively. For the E3 encounter (Figure 4), the negative water-cluster ions at discrete m/q values described by *Coates et al.* [2009] are clearly evident in the ELS spectrum; the positive molecular pick-up ions described by *Tokar et al.* [2009] are not evident in the IMS spectrum because they peaked 12 s (=173 km) earlier.

[7] Comparison of counting rates between adjacent angular sectors (not shown here) shows conclusively that

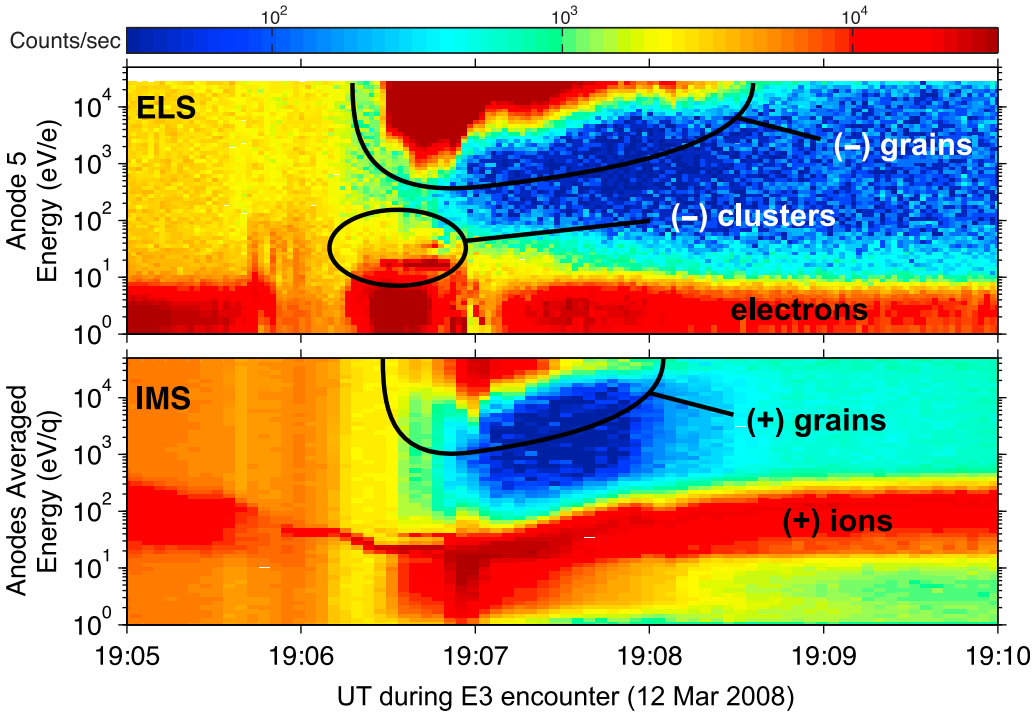

Figure 2. CAPS counting-rate spectrograms for the E3 Cassini encounter on 12 March 2008. The grain signatures at the highest energies are the subject of this paper. The diffuse background is due to penetrating energetic particles, which largely disappear during passage through the satellite's corotational wake.

the nanograins comprise highly collimated beams in the spacecraft reference frame, and hence represent cold populations that are almost at rest with respect to Enceladus [*Jones et al.*, 2009; *Tokar et al.*, 2009]. The observed shape of the E/q distribution is due almost entirely to the spacecraft ram velocity. (The spacecraft potential relative to the plasma is assumed here to be negligible, a perfectly adequate assumption for the signatures at $E/q > \sim 100$ eV/e considered

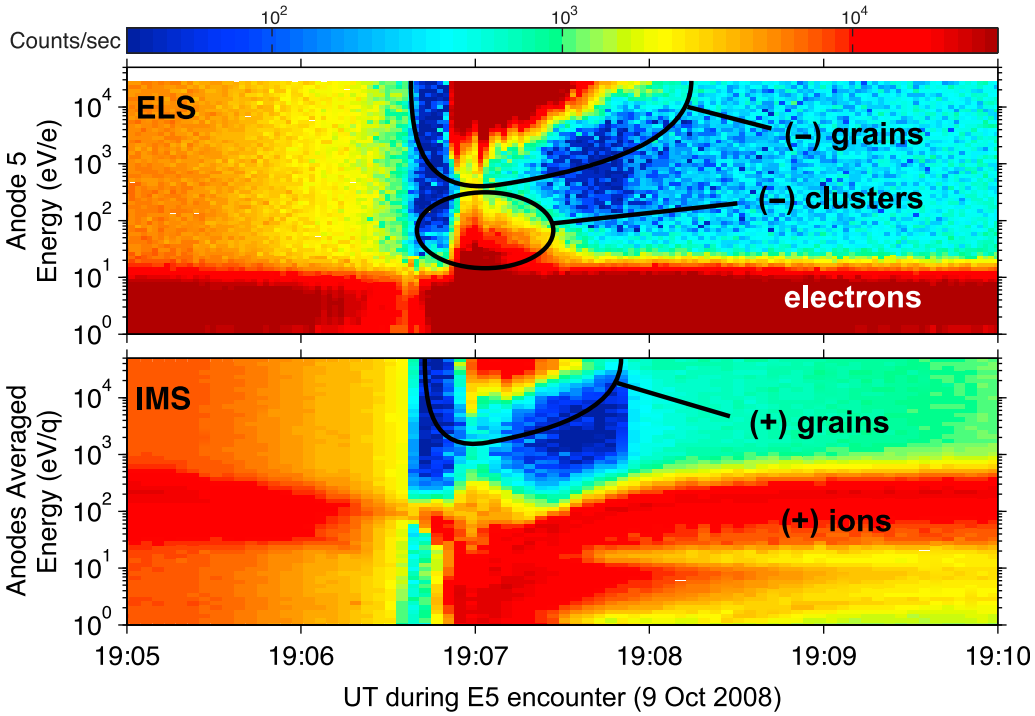

Figure 3. Same as Figure 2, but for the E5 encounter on 9 October 2008.

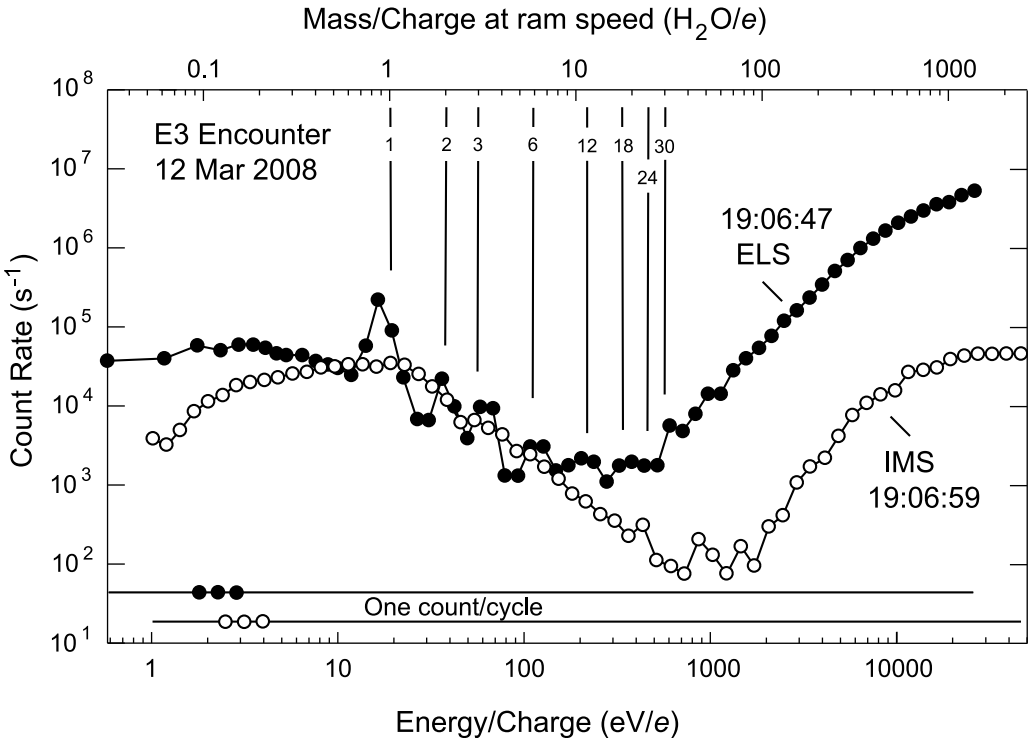

Figure 4. Counting rate spectra for negative (ELS) and positive (IMS) charged particles during the E3 encounter near the peak of the nanograin flux. The observed E/q range (bottom horizontal scale) is converted to m/q at the ram speed on the top horizontal scale, in units of water molecular masses per electronic charge.

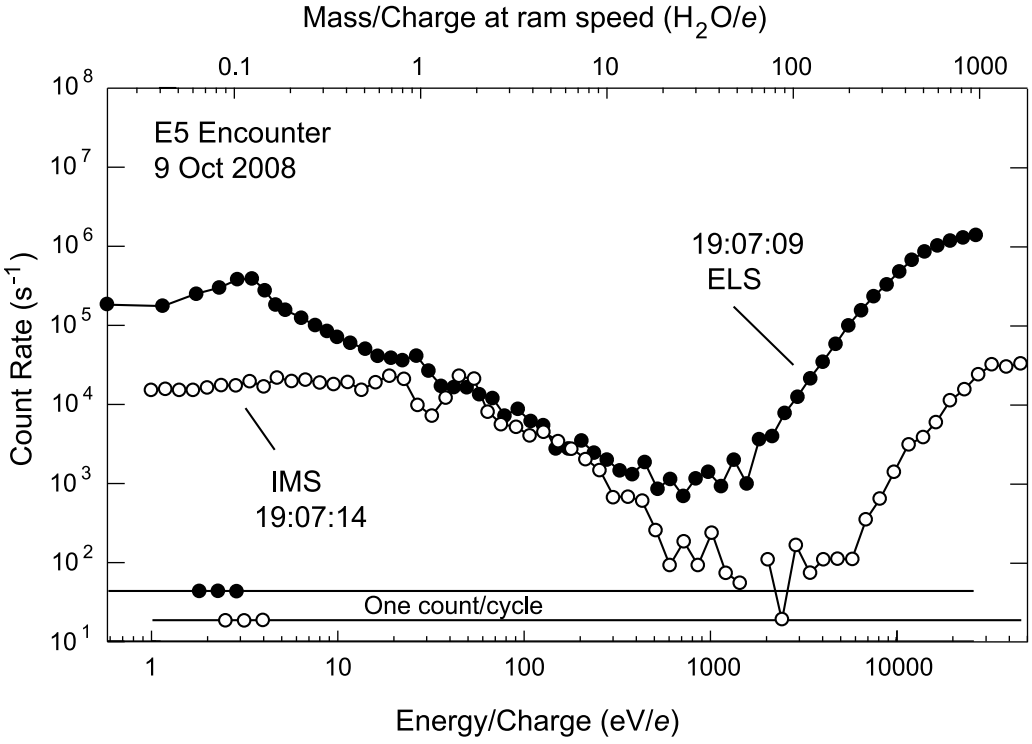

Figure 5. Same as Figure 4, for the E5 encounter.

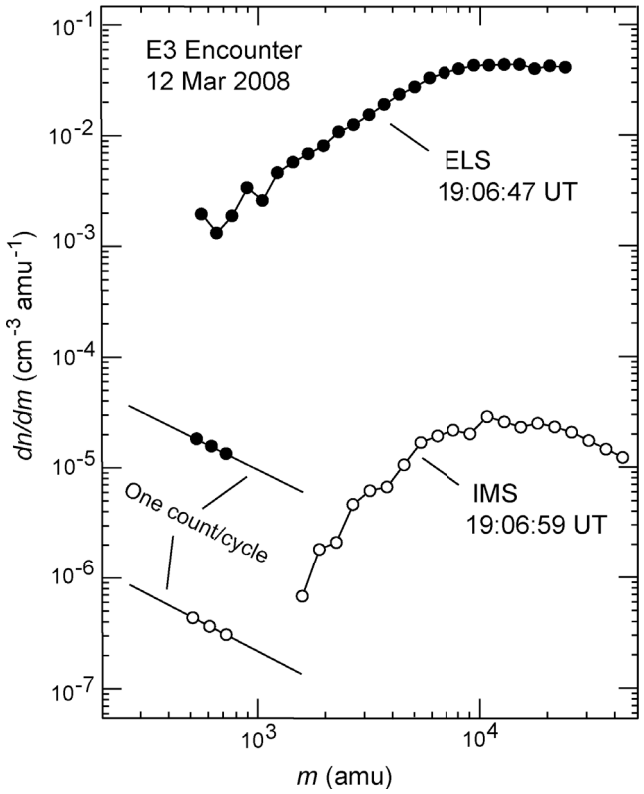

Figure 6. Charged nanograin number density per unit mass obtained from equation (1) with ELS and IMS counting rates near the times of the peak nanograin fluxes on the E3 encounter.

here.) The encounter speeds relative to Enceladus were $v = 14.4$, 17.7, and 7.7 km/s for E3, E5, and E7 respectively. These encounter speeds imply E/m conversion factors $v^2/2 = 1.1$, 1.6, and 0.31 eV/amu respectively. There is a small but unknown correction due to the beam speed relative to Enceladus, which is not measured. The fact that the beams appear in the nominal ram direction but not in adjacent sectors indicates that this correction, if known, would be small.

3. Density Distribution

[8] If the beam were to uniformly fill one particular angular sector of the instrument, it would be straightforward to compute the partial number density within each E/q channel (or, equivalently, each m/q channel) simply by multiplying the differential number flux in that sector by $v\Delta\Omega/2$ where $\Delta\Omega$ is the solid angle subtended by that sector. Summing these contributions over E/q channels would then provide an estimate of the total number density of particles within the CAPS E/q range that are visible in that angular sector.

[9] However, as noted above, comparison of adjacent sectors indicates that the beam's angular width is less than, and possibly much less than, the angular width of a sector, so this approach would yield only an upper limit, and possibly not a very close-upper limit, to the density. In this situation, a more accurate density determination is provided by the cold monoenergetic beam assumption employed by *Coates et al.* [2007] in their analysis of heavy negative ions in the atmosphere of Titan:

$$C(E/q) = \varepsilon n(E/q) v A \quad (1)$$

where $C(E/q)$ is the observed counting rate per E/q channel in the angular sector that includes the ram direction, ε is the detector counting efficiency (counts/particle), $n(E/q)$ is the number density of those particles that occupy the given E/q channel, v is the ram speed, and A is the collecting area per angular sector. For the collecting area we take $A = 0.33$ cm^2 both for ELS and IMS, which is subject to an uncertainty of perhaps a few tens of percent owing to the nonlinear response to a monoenergetic beam as a function of its location within the field of view of a given angular sector. An even larger uncertainty may apply to the counting efficiency ε, due primarily to uncertainty in the response of the micro-channel-plate detectors to slow heavy ions ($\gg$100 amu/e). For ELS we provisionally assume an efficiency $\varepsilon(-) \sim 0.05$ on the basis of laboratory measurements and modeling calculations presented by *Fraser* [2002]. This is uncertain by perhaps a factor $\sim$2–3, and may well depend on E/q, though it is taken here as a constant, lacking evidence to the contrary. For IMS we assume $\varepsilon(+) \approx 1$, with a smaller uncertainty, because the impact of such massive particles on the thin (0.5 μg/cm^2) carbon foils (present in IMS but absent in ELS) virtually assures the registration of one (and only one) start pulse and one end pulse in the counting circuit.

[10] Using these instrument parameters in (1) we derive the number density per unit mass dn/dm of charged nanograins shown in Figure 6 (for E3) and Figure 7 (for E5)

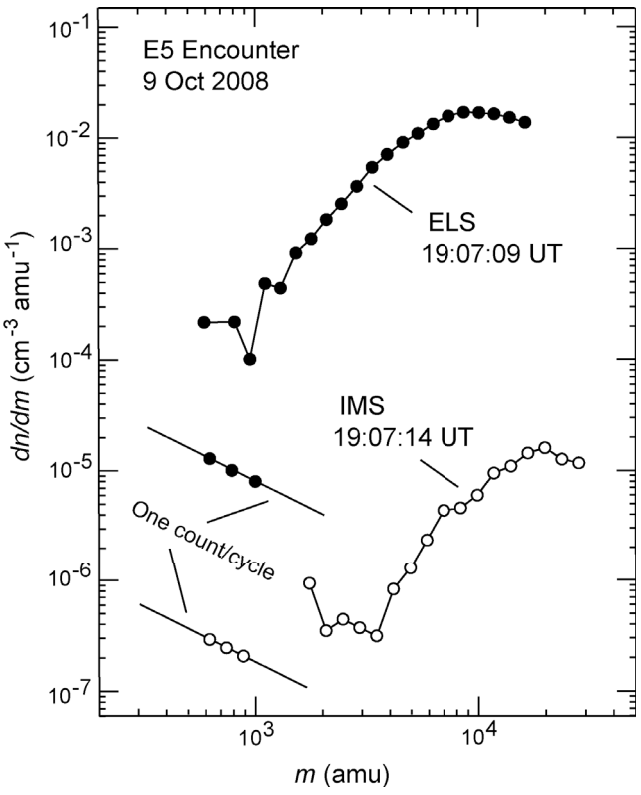

Figure 7. Same as Figure 6 for the E5 encounter.

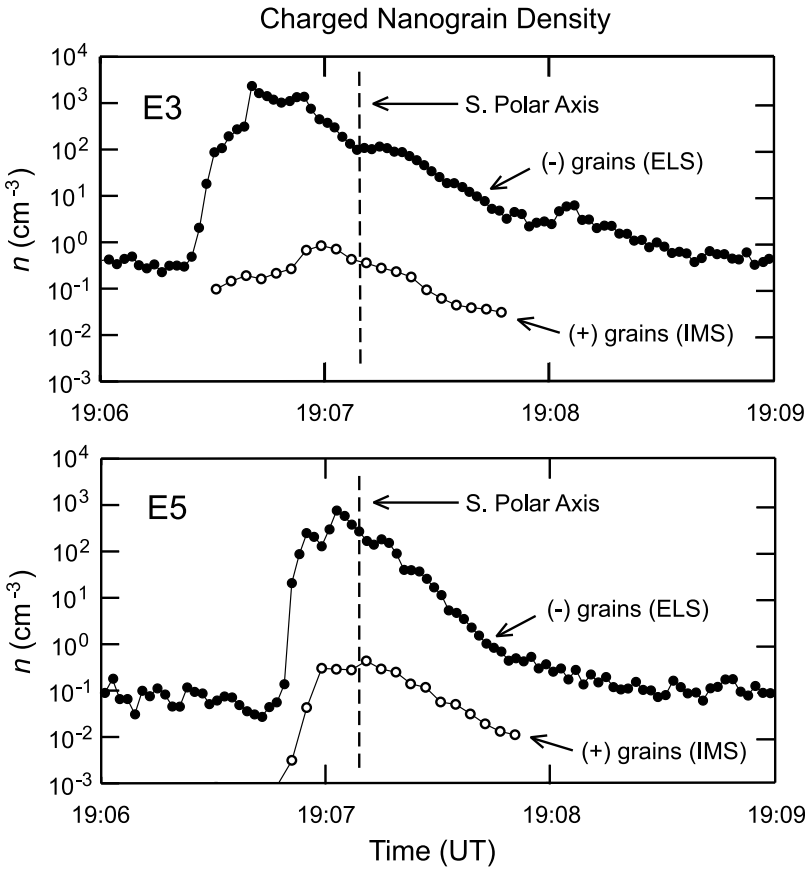

Figure 8. Total number densities of nanograins within the CAPS E/q (or m/q) ranges versus time during the (top) E3 and (bottom) E5 encounters. At each time step, the total density is obtained by integrating over dn/dm spectra like those shown in Figures 6 and 7. The vertical dashed line shows the time of the closest approach to the south polar axis of Enceladus, which occurred (by coincidence) at 19:07:09 UT for both encounters.

at the same sample times, near the nanograin flux peaks, shown in Figures 4 and 5 respectively. We assume here that the charge per grain is ± 1 e, as discussed in the section on "Implications for charging mechanisms" below. In these plots we include only those particles that are plausibly identifiable as nanograins in Figures 2 and 3 while excluding ambient plasma, locally produced molecular and cluster ions, and background counts. This provides the somewhat arbitrary but operationally sufficient criteria $m/q > 500$ amu/e for ELS and $m/q > 1700$ amu/e for IMS. Note that these spectra appear to have reached their peaks near the top end of the CAPS E/q range. Because we cannot determine the shape of the dn/dm spectra above the top of our E/q range, all we can say is that our measured charged nanograin densities are certainly less than, and possibly much less than, the total charged nanograin densities.

[11] Integrating over these dn/dm spectra gives the total charged nanograin number density within the CAPS E/q range for each spectrum. Repeating this for each of the many ($\sim$120) such spectra obtained during each encounter interval, we obtain the time series $n(t)$ shown in Figure 8. Maximum values are $n(-)$ $\sim$2600/cm^3 at 19:06:41 UT on E3 (Figure 8, top) and $\sim$760/cm^3 at 19:07:03 UT on E5 (Figure 8, bottom), and $n(+)$ $\sim$0.9/cm^3 (19:06:59 UT on E3) and $\sim$0.4/cm^3 (19:07:10 UT on E5). Notwithstanding the considerable uncertainties in the counting efficiencies noted after equation (1), there is no escaping the fact that the negative nanograins vastly outnumber the positive ones. Given the fact that each nanograin must carry at least ± 1 excess elementary charge in order to be detected by CAPS, it is also clear that the (net negative) charge density carried by such grains locally exceeds those (both positive and negative, presumably balanced) carried by the ambient plasma ($\sim$100/cm^3) in the Enceladus torus [*Thomsen et al.*, 2010]. It is, however, considerably less than the (oppositely unbalanced) peak charge density of the localized plume plasma during E3 as reported by *Shafiq et al.* [2011] and *Morooka et al.* [2011] on the basis of RPWS–LP data.

[12] In Figure 9 we show the mass density of the observed negative nanograins during the E3 encounter (solid curve), derived from Figure 8 (top) by multiplying the number density per E/q channel by the average particle mass per E/q channel before integrating over E/q. Shown for comparison is the mass density of the H_2O molecules measured simultaneously by the INMS instrument (dashed line) [*Dong et al.*, 2011]. Three things are worth noting: the timing of the nanograin density peak is roughly consistent with that of the H_2O vapor density peak; the width of the nanograin density peak is narrower than that of the H_2O vapor density

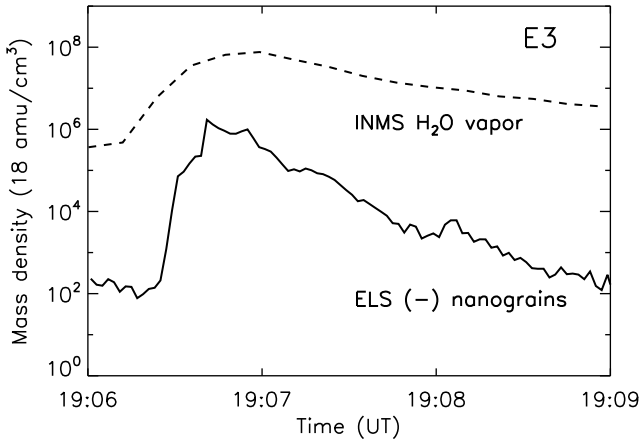

Figure 9. Mass densities of negatively charged nanograins measured by CAPS (solid curve) and of H_2O vapor molecules measured by INMS (dashed curve) during the E3 Cassini Enceladus encounter.

peak; and the nanograin mass density is consistently less than that of the H_2O molecules by a few orders of magnitude. Recall, however, that CAPS measurements provide only a lower limit, and perhaps not a very close lower limit, for the number density (hence mass density) of the nanograins. The higher m/q (higher E/q) nanograins, not measurable by CAPS, contribute more per particle to the mass density.

[13] For the later E7 encounter (2 Nov 2009) we do not have clear-cut results comparable to Figures 2–8 for E3 and E5, although E7 passed similarly close to the south polar axis at a distance much closer to the surface source, with the required CAPS ram pointing. (The south polar axis crossings of E3, E5, and E7 occurred at distances of 2.6, 1.3, and 0.4 R_E from the south-pole surface point, respectively, as indicated in Figures 1 and 10.) On E7, a positive nanograin signal was not detected by IMS. A negative nanograin signal was detected by ELS, but with a much lower signal-to-noise ratio than on the other two encounters. It was possible to calculate a total nanograin density profile from (1) analogous to Figure 8 which, although noisy, showed a distinct peak with maximum density of 1.4/cm^3 at 07:41:51 UT, very near the closest approach to the south polar axis. The qualitative appearance of the E7 ELS spectrogram was as if the ELS signatures in Figures 2 and 3 were displaced vertically upward, almost but not quite past the top of the ELS E/q range. This in spite of the fact that the ram speed on E7 (7.7 km/s) was considerably slower than that on E3 (14.4 km/s) or E5 (17.7 km/s), so that a given grain mass would produce a lower observed energy. We can speculate that only the larger nanograins have had time to acquire an excess electron at the closer position of the E7 encounter. We will argue below that the charging rate varies as the square of the grain dimension (7a,b) and hence as the 2/3 power of the grain mass (2).

[14] Including this ELS E7 data point, we show in Figure 10 a summary of the charged nanograin observations on the three encounters for which such measurements were enabled by the CAPS viewing direction. The ordinate is the maximum number density recorded during each encounter, and the abscissa is the corresponding distance from the surface of Enceladus (not from the center of Enceladus) along the south polar axis. Also shown for comparison is the $1/r^2$ dependence that would be expected for a flux-conserving expansion from a time-independent source. There is, of course, no reason to expect that the source is time-independent over intervals of several months, but it is worth noting that the neutral water-vapor component of the plume, as measured by INMS, was found to vary only by factors ~2 among these three encounters [*Dong et al.*, 2011] when extrapolated back to the source. By comparison, the neutral gas cloud model of *Smith et al.* [2010], integrated in time over several months, indicates a factor ~4 increase of the total source rate during the 7-month interval between E3 and E5.

4. Particle Size

[15] The conversion from observed E/q to intrinsic m/q is straightforward and probably correct, given that the particle speed relative to the spacecraft is dominated by the (known) spacecraft speed relative to Enceladus. To infer the particle mass we must assume something about its charge, and to convert mass to size we must further assume something about its density and structure.

[16] We assume that the bulk of the nanograins have either $q = 0$ (hence undetectable by CAPS), or $q = -1\ e$ (a single excess electron, hence detectable by ELS for sufficiently small m). For justification of this assumption please see the discussion in the following section. To convert mass to size, let us adopt the conventional assumption of compact spheres having the density and composition of water ice. The bulk water composition is confirmed by analysis of grain impacts on the INMS instrument [*Waite et al.*, 2009, supplemental information] and by analysis of the CDA results [*Postberg et al.*, 2011]. The assumption of compact spheres is probably

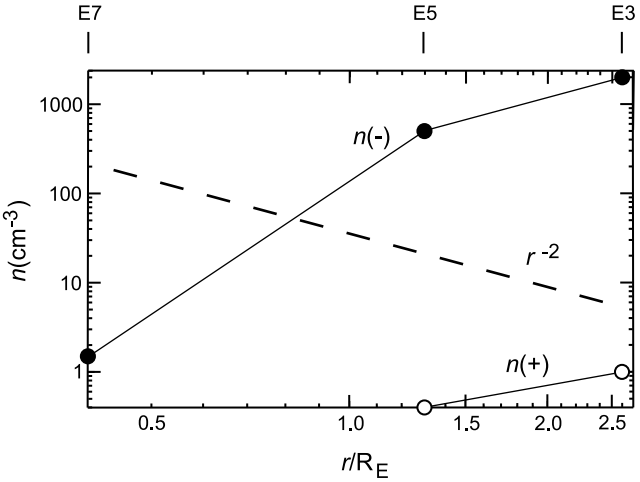

Figure 10. Maximum observed values of negatively and positively charged nanograin number density within the CAPS energy range observed during the three encounters analyzed here. The abscissa is distance from the south pole on the surface of Enceladus, not from the center of Enceladus. The nominal (flux-conserving) $1/r^2$ dependence is shown by the dashed line for comparison.

incorrect, but provides a useful lower limit for the particle size corresponding to a given particle mass. The conversion from mass m to radius a is then

$$\frac{a}{1\text{ nm}} > \left(\frac{m}{2500\text{ amu}}\right)^{1/3} \quad (2)$$

which represents a lower limit because a complex grain structure would be less dense than a compact sphere. The lower limit is, however, probably of the appropriate order of magnitude because it depends only on the 1/3 power of the density.

[17] As noted above, the encounter speeds were 14.4, 17.7, and 7.7 km/s, respectively, for the E3, E5, and E7 encounters. The top of the ELS E/q range (30 keV/e) then corresponds to masses up to 27000, 19000, and 97000 amu respectively (1500, 950, and 4900 H_2O molecular masses), or radii up to 2.2, 2.0, and 3.4 nm respectively. (Masses rounded to the nearest 1000 amu.) Thus, the designation "nanograin" is appropriate, and more specific than the more conventional "sub-micron grain" for the charged grains detectable by CAPS.

5. Implications for Charging Mechanisms

[18] Following the E3 and E5 encounters it was suggested [*Jones et al.*, 2009] that frictional (triboelectric) charging within the surface vents was a possible mechanism for charging the nanograins. Triboelectric charging can produce both negative and positive grains in comparable numbers, with negative charges favored for smaller particles and positive for larger ones [*Duff and Lacks*, 2008]. In situ plasma charging, by contrast, strongly favors negative grains for all particle sizes. In a quasi-neutral plasma the ambient electron flux typically exceeds the positive ion flux by the large factor $(m_i/m_e)^{1/2}$ at a given temperature, a factor ~43 for a hydrogen plasma or 182 for a water-ion plasma. The dense plume plasma reported by RPWS-LP is not quasi-neutral (see the second following paragraph below), but this is true only because the plasma electrons have already been largely attached to grains, both the nanograins reported here and the larger "sub-micron" grains that have been directly observed by the CDA instrument [*Kempf et al.*, 2008; *Postberg et al.*, 2011] and inferred from RPWS-LP measurements [*Farrell et al.*, 2010; *Shafiq et al.*, 2011]. Thus the conclusion remains that in situ plasma charging strongly favors the production of negative grains.

[19] The analysis shown here strongly favors the in situ charging hypothesis for three reasons: (1) the negative grains do indeed greatly outnumber the positive ones (Figures 4–8), as expected for in situ plasma charging; (2) the trend shown in Figure 10 strongly suggests that the nanograins leave Enceladus largely uncharged, thus explaining their relatively weak signal in ELS and the absence of a signal in IMS on the much closer E7 encounter; and (3) electron-impact charging becomes much faster, and hence more viable, in light of the very dense plume plasma reported by *Shafiq et al.* [2011] and *Morooka et al.* [2011] on the basis of RPWS–LP data.

[20] The density peak of the LP plasma ions [*Shafiq et al.*, 2011, Figure 2] closely resembles, in location and shape, the density peak of the negative nanograins shown in Figure 8 (top) for the same encounter. Moreover, the LP plasma data indicate a strong charge density imbalance of the opposite sense to that indicated by the nanograin data: $n(+) \gg n(-)$ for the plasma and vice versa for the nanograins. Taken in isolation, either of these results might be suspect because charge quasi-neutrality is enforced quite rigorously on spatial scales ≫ the Debye length and time scales ≫ the electron plasma period, both of which conditions are easily satisfied on the spatial and temporal scales of these measurements. Taken together, however, the two results are quite compatible; indeed, they require each other for consistency. In fact, the presence of sub-micron-sized grains in the plume has already been inferred [*Farrell et al.*, 2009, 2010; *Wahlund et al.*, 2009; *Shafiq et al.*, 2011; *Morooka et al.*, 2011] as needed to explain the LP result $n(+) \gg n(-)$. It seems quite plausible that the nanograins carry a significant fraction of the negative charge in the dusty plasma environment of the plume. The numbers do not match in detail: $n(+) - n(-) \sim 10^4/\text{cm}^3$ for the LP plume plasma on E3, versus $n(-) - n(+) \sim 10^3/\text{cm}^3$ for the nanograins near the respective peaks. However, we have already noted above that CAPS can detect only a fraction (perhaps a small fraction) of the charged grains because they extend well off the top of the CAPS E/q range. Similar charge-density imbalances, with $n(+) > n(-)$, are seen by the RPWS-LP on other plume encounters, but the analysis of these other encounters is still a work in progress.

[21] We suggest that the most likely (nonzero) charge on each nanograin is $q = -1\ e$ (a single excess electron), for three independent reasons. First, a purely statistical reason: if the probability of acquiring a single excess electron through inelastic collisions is $p < 1$, then the probability of acquiring n excess electrons, even ignoring electrostatic repulsion, is $p^n < p$. Second, an empirical reason: if there were a significant abundance of multiply charged grains one would expect, for each singly charged m/q peak, a series of ghost peaks at integral fractions (1/2, 1/3, etc.) of the main m/q peak value, and these are not observed. This argument is particularly compelling for the well-resolved m/q peaks of the smaller negative cluster ions evident in Figure 4 (top horizontal scale) below ~20 H_2O molecular masses per elementary charge.

[22] The third reason is physical: each electron attached to a grain makes it less likely that another will be attached, because of electrostatic repulsion. The extreme case of this is the steady state equilibrium grain potential, where the grain is sufficiently charged to repel the entire thermal electron flux (minus the much smaller positive ion flux) by Debye shielding. For a Maxwellian electron velocity distribution in an O^+-dominated plasma this equilibrium potential is

$$\phi_{eq} \approx -3.6kT_e/e \sim -10\text{V} \quad (3)$$

independent of grain size [e.g., *Horányi*, 1996], corresponding to an equilibrium grain charge

$$q_{eq} = 4\pi\varepsilon_o a \ \ \phi_{eq} \sim -7e(a/1\text{ nm}) \quad (4)$$

This is too large to be relevant to limiting the grain charge to $-1\ e$ for nm-size grains. But there is a more stringent upper limit imposed by field emission, where the electrostatic repulsion potential between two neighboring excess electrons exceeds their work function in the material of the grain. For

compact spherical ice grains the field emission limiting potential is

$$\phi_{fe} \approx -1\mathrm{V}(a/1\ \mathrm{nm}) \tag{5}$$

[*Mendis and Axford*, 1974], corresponding to a limiting grain charge

$$q_{fe} \sim -0.7e(a/1\ \mathrm{nm})^2 \tag{6}$$

which is clearly relevant for nm-size grains. This limit will be even smaller if the grain is neither compact nor spherical, as seems likely. We propose that the effective limit for nm-sized grains is -1 *e* (a single excess electron cannot repel itself).

[23] Any one of the above three arguments taken alone might be considered less than compelling. Taken together, however, they strongly support the conclusion that $q = -1$ *e* is the most likely charge state, if not the only stable charge state, of the nanograins measured by CAPS on these three encounters. It is worth noting that the field-emission limit (6) is less than the Debye-shielding limit (4) for grain radii less than ~10 nm, which includes all grains detectable by CAPS on these encounters. Such particles, however long they are exposed to the plasma, are incapable of holding a fully developed Debye sphere. The limitation to one excess electron applies to grain sizes less than a few nm (cf. equations (2) and (6)), not to the larger sub-micron and micron-size grains observed by the CDA [*Kempf et al.*, 2008; *Postberg et al.*, 2011] and invoked to explain the non-neutral plume plasma observed by the RPWS-LP [*Farrell et al.*, 2009; *Shafiq et al.*, 2011].

[24] Finally, let us estimate the time and space scales relevant to grain charging by electron attachment in the plume environment. A spherical grain with radius *a* has a surface area $S = 4\pi a^2$ available to intercept an isotropic electron flux, assuming unit sticking efficiency. (The sticking efficiency may well be <1 or even ≪ 1, but this does not affect the comparisons below if the sticking efficiency is independent of the grain size and of distance from Enceladus.) The plasma has a thermal electron flux $F_e = n_e(kT_e/m_e)^{1/2}$ and a positive ion flux that is typically (and evidently in this case) much smaller. For the ambient Enceladus torus plasma ($n_e \sim 100/\mathrm{cm}^3$, $T_e \sim 3$ eV), $F_e \sim 7 \times 10^9$ /cm^2-s. For the dense plume plasma reported by *Shafiq et al.* [2011] for E3, n_e is perhaps 10 × larger while T_e is perhaps of the same order of magnitude, resulting in a ~10 × enhancement of the electron thermal flux. Then the electron impact rate on a grain would be

$$R_T = F_e S \sim \left(9 \times 10^{-4}/s\right)\left(\frac{a}{1\ \mathrm{nm}}\right)^2 \tag{7a}$$

in the ambient torus plasma, or

$$R_P = F_e S \sim \left(9 \times 10^{-3}/s\right)\left(\frac{a}{1\ \mathrm{nm}}\right)^2 \tag{7b}$$

in the enhanced plume plasma.

[25] The mean free path for a grain against electron impact is $\lambda = v/R$ where *v* is the grain speed relative to Enceladus. As noted above, *v* is not measured, but we can put plausible limits on it. It is presumably at least of the order of the surface escape speed from Enceladus (239 m/s) or the grain would not have reached the point of observation ~1 R_E away. And it is presumably less than the flow speed of the neutral water vapor escaping the vents because the gas flow is presumably driving the grain flow, not vice versa. By fitting a supersonic expansion model to the INMS gas density data from the three encounters analyzed here, *Dong et al.* [2011] obtain a gas flow speed in the range 500–800 m/s for all three encounters. Thus, assuming $v \sim 500$ m/s for the grain speed, we obtain a mean free path λ for a grain of radius *a*

$$\lambda_T = v/R_T \sim (2\ \mathrm{R_E})\left(\frac{1\ \mathrm{nm}}{a}\right)^2 \tag{8a}$$

in the ambient torus plasma, or

$$\lambda_P = v/R_P \sim (0.2\ \mathrm{R_E})\left(\frac{1\ \mathrm{nm}}{a}\right)^2 \tag{8b}$$

in the enhanced plume plasma reported for E3. Thus, even in the ambient plasma environment, it is not unlikely that a nanograin will have acquired one excess electron within the distance of the E3 and E5 plume axis encounters (2.6 and 1.3 R_E respectively), and it is quite likely in the enhanced plume plasma environment. It is even possible that the size dependence in (8a) and (8b) could explain the positive slope of the nanograin spectra in Figures 4–7. Smaller grains may well be present in greater numbers, but have had insufficient time to acquire even a single excess electron from the resident plasma.

[26] The existence of a relatively small but measurable nonzero flux of positive nanograins on E3 and E5 requires a different charging mechanism, of course. One possibility is that a small fraction of the impacting electrons have sufficient energy to liberate more than one secondary electron. Another possibility is the relatively small but nonzero flux of positive ions impacting the grains. A third possibility, as suggested by *Jones et al.* [2009], is triboelectric charging before escape.

[27] There is obviously much theoretical work to be done in quantitative modeling of the chemical and electrodynamic interactions between the nanograins and the plasma. For example, the thermal electron flux of the plume plasma is probably a strong function of distance from the source, because the plume plasma is probably created by impact ionization of the escaping water vapor, first by the ambient plasma and ultimately by the plume plasma itself in a bootstrap process. Nevertheless, the above simple calculation serves to illustrate that electron impact charging from the observed plasma is quite sufficient to explain the presence of (mostly negative) charged nanograins in the plume. Additional encounter observations will be very helpful, of course.

6. Timing Difference Between Negative and Positive Grain Signatures

[28] There is a clear and consistent timing difference between the sudden encounters with the negative and positive grain signatures on both E3 and E5; see Figures 2, 3, and 8. The negative (ELS) grain signature precedes the positive (IMS) grain signature on both encounters. The suddenness of the encounters is puzzling in itself. The timing of these

encounters bears no obvious relationship to the encounter geometry – both are already well within the magnetic flux tube that would intersect Enceladus, assuming a north-south field orientation. Nor is there any obvious reason why that flux tube boundary would even matter to these high m/q particles that are not yet magnetically trapped. Moreover, the direction of the offset between negative and positive grain distributions is puzzling. It cannot be explained simply in terms of electrostatic deflection by the remnant corotation electric field, which has a positive radial component, and these are both inbound encounters. If the timing difference were produced by electric field deflection, the positive grains should appear before the negative ones, not after as observed. We do not understand these encounter timing details, but we consider them worth mentioning as topics for future study.

7. Conclusions

[29] During three ram-pointing encounters with the Enceladus south polar plumes, the Cassini Plasma Spectrometer has analyzed a new class of charged particles, nanometer-sized water ice grains. The E/q range of the CAPS detectors, coupled with the spacecraft encounter speeds, limits our detection to m/q values below $\sim 10^4$–10^5 amu/e for the three available encounters, corresponding to ~1000–5000 H_2O molecular masses per elementary charge, but the resident particle distribution clearly extends to much higher m/q values that cannot be detected by CAPS.

[30] We have argued that the most likely nonzero charge per grain is ± 1 e, with negative grains outnumbering positive ones by a factor ~2000–3000 within the CAPS E/q range, as required by the observations. We have also argued that this result is consistent with the idea that the nanograins leave Enceladus largely uncharged, and become increasingly negatively charged as they move away from Enceladus by attachment of electrons from the plume plasma. The nanograins are significant carriers of negative charge away from Enceladus, and the implied electric current is evidently closed by the simultaneous escape of a dense plume plasma which has the opposite sign of (+) net charge density [*Shafiq et al.*, 2011; *Morooka et al.*, 2011]. If this return current is not spatially coincident with the nanograin current, the implied current loop may have significant effects on the magnetic perturbations that have been observed on these and many other Enceladus encounters by the Cassini magnetometer [*Khurana et al.*, 2007], as discussed recently by *Simon et al.* [2011]. In addition to the implied electric current system, there are many other remaining questions to be answered relating to the subsequent dynamics and resulting spatial distribution of the nanograins, and their intimate coupling with the plasma and neutral gas. They undoubtedly make important contributions to the localized source of material for the Enceladus plasma torus and the E ring.

[31] The ultimate fate of these charged nanograins is an open question. It is possible that, following acceleration by the rotational electric field, they contribute to the flux of small fast grains observed by CDA in the Enceladus torus [*Kempf et al.*, 2008] and in interplanetary space [*Kempf et al.*, 2005a, 2005b]. It is clear that we have much to learn about this novel phenomenon through further analysis of this data set and future close encounters of the Enceladus plume.

[32] **Acknowledgments.** We thank the two reviewers for their helpful comments. This work was supported in part by NASA JPL contracts 1243218 and 1405851 to the Southwest Research Institute. Work at Los Alamos was conducted under the auspices of the U.S. Department of Energy, with support from NASA's Cassini project. Work at Mullard was supported by STFC (United Kingdom) and by ESA through the U.K. Space Agency. G.H.J. is supported by an STFC Advanced Fellowship. Work at the University of Colorado was supported by the NASA Cassini Data Analysis Program. The RPWS–LP efforts are supported by the Swedish National Space Board (SNSB).

[33] Masaki Fujimoto thanks the reviewers for their assistance in evaluating this paper.

References

Coates, A. J., F. J. Crary, G. R. Lewis, D. T. Young, J. H. Waite Jr., and E. C. Sittler Jr. (2007), Discovery of heavy negative ions in Titan's ionosphere, *Geophys. Res. Lett.*, *34*, L22103, doi:10.1029/2007GL030978.

Coates, A. J., G. H. Jones, G. R. Lewis, A. Wellbrock, D. T. Young, F. J. Crary, R. E. Johnson, T. A. Cassidy, and T. W. Hill (2009), Negative ions in the Enceladus plume, *Icarus*, *206*, 618–622, doi:10.1016/j.icarus.2009.07.013.

Coates, A. J., A. Wellbrock, G. R. Lewis, G. H. Jones, D. T. Young, F. J. Crary, J. H. Waite, R. E. Johnson, T. W. Hill, and E. C. Sittler Jr. (2010), Negative ions at Titan and Enceladus: Recent results, *Faraday Discuss.*, *147*, 293–305, doi:10.1039/c004700g.

Dong, Y., T. W. Hill, B. D. Teolis, B. A. Magee, and J. H. Waite (2011), The water vapor plumes of Enceladus, *J. Geophys. Res.*, *116*, A10204, doi:10.1029/2011JA016693.

Duff, N., and D. J. Lacks (2008), Particle dynamics simulations of triboelectric charging in granular insulator systems, *J. Electrost.*, *66*, 51–57, doi:10.1016/j.elstat.2007.08.005.

Farrell, W. M., W. S. Kurth, D. A. Gurnett, R. E. Johnson, M. L. Kaiser, J.-E. Wahlund, and J. H. Waite Jr. (2009), Electron density dropout near Enceladus in the context of water-vapor and water-ice, *Geophys. Res. Lett.*, *36*, L10203, doi:10.1029/2008GL037108.

Farrell, W. M., W. S. Kurth, R. L. Tokar, J.-E. Wahlund, D. A. Gurnett, Z. Wang, R. J. MacDowall, M. W. Morooka, R. E. Johnson, and J. H. Waite Jr. (2010), Modification of the plasma in the near-vicinity of Enceladus by the enveloping dust, *Geophys. Res. Lett.*, *37*, L20202, doi:10.1029/2010GL044768.

Fraser, G. W. (2002), Ion detection efficiency of microchannel plates (MCPs), *Int. J. Mass Spectrom.*, *215*, 13–30, doi:10.1016/S1387-3806(01)00553-X.

Hansen, C. J., L. Esposito, A. I. F. Stewart, J. Colwell, A. Hendrix, W. Pryor, D. Shemansky, and R. West (2006), Enceladus' water vapor plume, *Science*, *311*, 1422–1425, doi:10.1126/science.1121254.

Horányi, M. (1996), Charged dust dynamics in the solar system, *Annu. Rev. Astron. Astrophys.*, *34*, 383–418, doi:10.1146/annurev.astro.34.1.383.

Jones, G. H., et al. (2009), Fine jet structure of electrically charged grains in Enceladus's plume, *Geophys. Res. Lett.*, *36*, L16204, doi:10.1029/2009GL038284.

Kempf, S., R. Srama, M. Horányi, M. Burton, S. Helfert, G. Moragas-Klostermeyer, M. Roy, and E. Grün (2005a), High-velocity streams of dust originating from Saturn, *Nature*, *433*, 289–291, doi:10.1038/nature03218.

Kempf, S., et al. (2005b), Composition of saturnian stream particles, *Science*, *307*, 1274–1276, doi:10.1126/science.1106218.

Kempf, S., U. Beckmann, G. Moragas-Klostermeyer, F. Postberg, R. Srama, T. Economou, J. Schmidt, F. Spahn, and E. Grün (2008), The E ring in the vicinity of Enceladus 1. spatial distribution and properties of the ring particles, *Icarus*, *193*, 420–437, doi:10.1016/j.icarus.2007.06.027.

Khurana, K. K., M. K. Dougherty, C. T. Russell, and J. S. Leisner (2007), Mass loading of Saturn's magnetosphere near Enceladus, *J. Geophys. Res.*, *112*, A08203, doi:10.1029/2006JA012110.

Mendis, D. A., and W. I. Axford (1974), The dynamics of micrometeoroids in planetary magnetospheres, *Annu. Rev. Earth Planet. Sci.*, *2*, 419–474, doi:10.1146/annurev.ea.02.050174.002223.

Morooka, M. W., J.-E. Wahlund, A. I. Eriksson, W. M. Farrell, D. A. Gurnett, W. S. Kurth, A. M. Persoon, M. Shafiq, M. André, and M. K. G. Holmberg (2011), Dusty plasma in the vicinity of Enceladus, *J. Geophys. Res.*, *116*, A12221, doi:10.1029/2011JA017038.

Porco, C. C., et al. (2006), Cassini observes the active south pole of Enceladus, *Science*, *311*, 1393–1401, doi:10.1126/science.1123013.

Postberg, F., J. Schmidt, J. Hillier, S. Kempf, and R. Srama (2011), A salt-water reservoir as the source of a compositionally stratified plume on Enceladus, *Nature*, *474*, 620–622, doi:10.1038/nature10175.

Shafiq, M., J.-E. Wahlund, M. W. Morooka, W. S. Kurth, and W. M. Farrell (2011), Characteristics of the dust-plasma interaction near Enceladus' south pole, *Planet. Space Sci.*, *59*, 17–25, doi:10.1016/j.pss.2010.10.006.

Simon, S., J. Saur, H. Kriegel, F. M. Neubauer, U. Motschmann, and M. K. Dougherty (2011), Influence of negatively charged plume grains and hemisphere coupling currents on the structure of Enceladus' Alfvén wings: Analytical modeling of Cassini magnetometer observations, *J. Geophys. Res.*, *116*, A04221, doi:10.1029/2010JA016338.

Smith, H. T., R. E. Johnson, M. E. Perry, D. G. Mitchell, R. L. McNutt, and D. T. Young (2010), Enceladus plume variability and the neutral gas densities in Saturn's magnetosphere, *J. Geophys. Res.*, *115*, A10252, doi:10.1029/2009JA015184.

Spahn, F., et al. (2006), Cassini dust measurements at Enceladus and implications for the origin of the E ring, *Science*, *311*, 1416–1418, doi:10.1126/science.1121375.

Spencer, J. R., J. C. Pearl, M. Segura, F. M. Flasar, A. Mamoutkine, P. Romani, B. J. Buratti, A. R. Hendrix, L. J. Spilker, and R. M. C. Lopes (2006), Cassini encounters Enceladus: Background and the discovery of a south polar hot spot, *Science*, *311*, 1401–1405, doi:10.1126/science.1121661.

Thomsen, M. F., D. B. Reisenfeld, D. M. Delapp, R. L. Tokar, D. T. Young, F. J. Crary, E. C. Sittler, M. A. McGraw, and J. D. Williams (2010), Survey of ion plasma parameters in Saturn's magnetosphere, *J. Geophys. Res.*, *115*, A10220, doi:10.1029/2010JA015267.

Tokar, R. L., R. E. Johnson, M. F. Thomsen, R. J. Wilson, D. T. Young, F. J. Crary, A. J. Coates, G. H. Jones, and C. S. Paty (2009), Cassini detection of Enceladus' cold water-group plume ionosphere, *Geophys. Res. Lett.*, *36*, L13203, doi:10.1029/2009GL038923.

Wahlund, J.-E., et al. (2009), Detection of dusty plasma near the E-ring of Saturn, *Planet. Space Sci.*, *57*, 1795–1806, doi:10.1016/j.pss.2009.03.011.

Waite, J. H., Jr., et al. (2006), Cassini Ion and Neutral Mass Spectrometer: Enceladus plume composition and structure, *Science*, *311*, 1419–1422, doi:10.1126/science.1121290.

Waite, J. H., Jr., et al. (2009), Liquid water on Enceladus from observations of ammonia and ^{40}Ar in the plume, *Nature*, *460*, 487–490, doi:10.1038/nature08153.

Young, D. T., et al. (2004), Cassini Plasma Spectrometer investigation, *Space Sci. Rev.*, *114*, 1–4, doi:10.1007/s11214-004-1406-4.